A mixed hexahedral finite element to model the scattering of a deformed microstrip antenna

Nicolas Adnet, Isabelle Bruant, F. Pablo, Laurent Proslier

A mixed hexahedral finite element to model the scattering of a deformed microstrip antenna

N. Adnet, I. Bruant, F. Pablo, and L. Proslier

Laboratoire d'Energétique, Mécanique et Electromagnétisme, Université Paris Ouest Nanterre La Défense, Ville d'Avray, France

ABSTRACT

Microstrip antennas have a major interest in aeronautical applications due to their low profile. This paper deals with the impact of mechanical strain on the scattering properties of these antennas. Considering a weak coupling between electromagnetism and mechanical behavior, the same 3D hexahedral finite element discretization is used to solve both problems. A node-based approximation is used for mechanical displacement, while for the determination of the electromagnetic fields, a vector finite approximation is implemented to ensure a better consideration of electromagnetic boundary conditions. The weak electromagnetic formulation inducing integrals on open infinite domains, a Boundary Integral Method is used.

KEYWORDS

Boundary integral method; electromagnetic/mechanical coupling; finite element method; Maxwell's equations; microstrip antenna; scattering; vector finite element

1. Introduction

Due to increasing needs in navigation, communication and surveillance, aircrafts are equipped with more and more antennal structures. The antennas implementation have drastic backlashes on aircrafts design. Indeed, antennas reduce aircraft aerodynamic efficiency, lead to structural weakening (drillings), cannot be placed anywhere and induce a weight increase through wiring. Thus, the decrease of antennas number and locations on future aircrafts is a crucial stake in aeronautics.

Many researches focused on embedding antennas on aircraft structural surfaces (fuselage, wings, tail, ...) have been performed over the last 15 years in order to improve both structural efficiency and antenna performances [1]. These studies especially led in the development of microstrip antennas which are low profile and conformable to planar and warped surfaces. Hence, these antennas can easily be bounded on aircraft structural surfaces. Moreover, the emergence of metamaterials (new electromagnetic materials) will soon allow us to elaborate multifrequencies microstrip antennas.

In flight conditions, planes are subjected to aerodynamic loads leading to the structure distortion. Hence, the influences of the structural surfaces distortions on the microstrip electromagnetic response have to be studied, independently of antenna developments. The knowledge of mechanical strains could then be used for smart tuning of the antennas.

A few papers dealing with curved antennas can be found in the literature. In Antilla and Alexopoulos [2], a 3D hybrid finite element-integral equation method has been developed in general curvilinear coordinates. In Jacobs [3], planar and curved radiative microstrip antennas are, for example, analyzed. The influence of the curvature on the radar cross section (RCS) is moreover shown for such antennas in Volakis et al. [4]. Nevertheless, for cavities antennas, only simple configurations like cylindrical surfaces are considered in these works. In operating conditions, the strained surfaces of the antenna being complex, specific tools have to be developed. On an other hand, an overview of industrial coupling softwares (such as ANSYS, COMSOL) has shown that these tools are not well suited to solve this kind of coupled problem [5] and [6]. The novelty of this work is to mix the mechanical and electromagnetic problems using the same finite element in order to take into account the physical distortion of the antenna.

The present work, focused on the development of a numerical tool able to predict the impact of microstrip distortions on electromagnetic fields, is part of the MSIE project (Intelligent Materials and Structures for Electromagnetism), launched in 2008 by the competitiveness french cluster AStech with the view of answering to the above problematic.

This paper presents the study of electromagnetic/mechanical coupling modeling for the analysis of microstrip antennas scattering. It derives from usual mechanical approach and specific mathematic tools for free space problems [4], [7]. From a 3D discretization of the structure, a classical mechanical finite nodal element model is coupled with an electromagnetic finite vector element one, developed by Jin [8]. This leads to a particular finite element having both nodal mechanical and edges electromagnetic degrees of freedom. Hence, the electromagnetic/mechanical problem is solved using the same mesh. In order to solve mechanical problems with warped or distorted antennas, the considered finite element is an hexahedral one. Using the usual boundary integral method, the electromagnetic fields are obtained in the whole space.

In a first part, the microstrip antenna integrated on a composite structure is described and the governing equations are detailed. The finite element approximation is presented in the second part and deals with the electromagnetic field

CONTACT Dr. F. Pablo fredericrf.01sirap-u@olbap. Laboratoire d'Energétique, Mécanique et Electromagnétisme, Université Paris Ouest Nanterre La Défense, EA

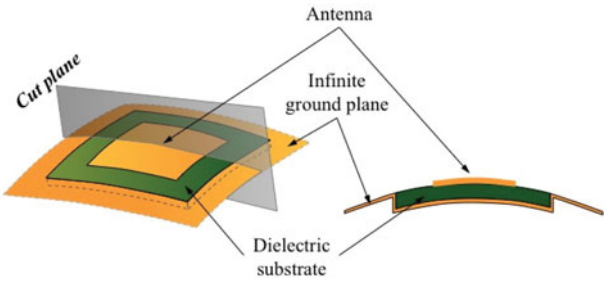

Figure 1. The studied structure.

approximation, using the finite vector element approach and the boundary integral method. In the last section, this recent numerical tool is used through various configurations.

2. Problem description

2.1. *Geometric description*

The specific structure to be considered in the present work is illustrated in Figure 1. It consists in a rectangular microstrip patch antenna printed on a dielectric substrate. A ground plane is glued underneath the substrate in order to stop electromagnetic waves propagation. The antenna thickness being far smaller than the substrate one, it will be neglected in the following developments. This structure is then supposed to be integrated on composite aircraft panels.

The cavity model, described in Jin [8] and illustrated in Figure 2 can be used to represent the above structure. The ground plane is then considered as an infinite metallic plane and the substrate is attended in all the cavity.

In the following developments, the infinity space located above the cavity and the ground plane, and the inside of the cavity will, respectively, be represented by V_∞ and V symbols.

Studying the antenna scattering, the cavity is assumed to be subjected to electromagnetic waves emitted by a source point of V_∞.

Considering the Cartesian coordinate system $(O, \hat{x}, \hat{y}, \hat{z})$ presented in Figure 3

- any observation point $M(x, y, z)$ of the infinity space is located by the vector $\vec{r} = \overrightarrow{OM}$ whose euclidian norm is defined by $r = \|\vec{r}\| = \sqrt{x^2 + y^2 + z^2}$, (note that M is located by $M(r, \theta, \phi)$ in the spherical frame $(\hat{\rho}, \hat{\theta}, \hat{\phi})$);

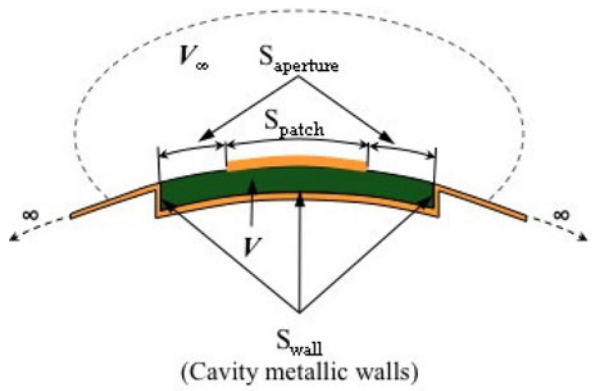

Figure 2. The cavity model.

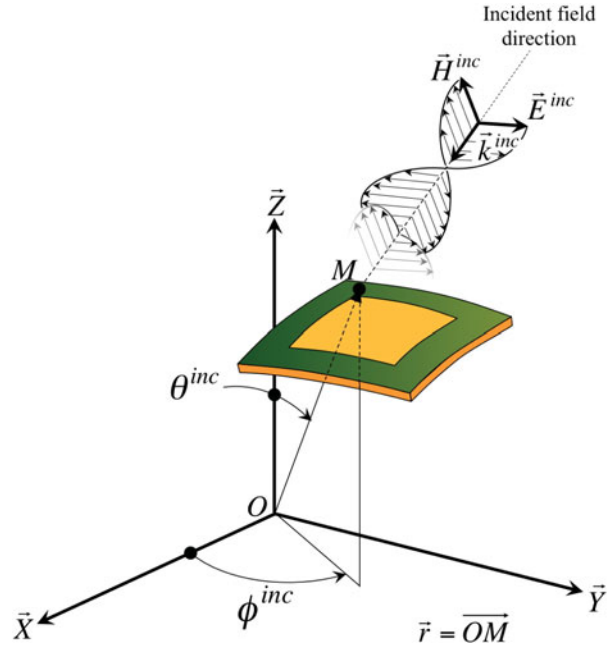

Figure 3. The coordinate system.

- the $\vec{E}^{inc}$ and $\vec{H}^{inc}$ field are emitted from a source point M', located by $\vec{r}' = \overrightarrow{OM'}$, and received by the observation point M.

Finally, it is assumed that the cavity is subjected to mechanical strains and loads. The governing equations and variational formulations are presented in the next subsections.

2.2. *Mechanical governing equations and weak form*

As previously underlined, the structural cavity V will be bounded on composite panels which are distorted by external loads. Hence, this distortion will affect V. The study of its mechanical strains is then essential.

Considering a static approach, the mechanical governing equations consists in the equilibrium equation, the constitutive equation in V and the strain-displacement relationship [9]:

$$\overrightarrow{div}\,\mathbf{T} + \vec{f} = \vec{0}, \tag{1}$$

$$\mathbf{T} = \mathrm{a}\,\mathbf{S}(\vec{u}), \tag{2}$$

$$\mathbf{S}(\vec{u}) = \frac{1}{2}(\mathbf{grad}\,\vec{u} + \mathbf{grad}^T\vec{u}), \tag{3}$$

where $\mathbf{T}$, $\mathbf{S}(\vec{u})$, $\vec{f}$ and a are, respectively, the stress tensor, the strain tensor, the prescribed body forces vector applied to V and the elastic stiffness tensor. In addition to these equations, one has to take into account the mechanical boundary conditions: a first one where mechanical vector displacement $\vec{u}$ is imposed, and the second one where a surface force vector $\vec{F}$ is applied on the boundary ∂V_F.

The classical weak form of the mechanical problem is then given by the following:

Find $\vec{u} \in \mathcal{U}_{ad}$ such that

$$\int_V \mathbf{S}^*(\vec{u}^*) : \mathbf{T}(\vec{u})\,dV = \int_V \vec{u}^*.\,\vec{f}\,dV + \int_{\partial V_F} \vec{u}^*.\,\vec{F}\,dS, \tag{4}$$

for any admissible virtual displacement $\vec{u}^* \in \mathcal{U}^*_{ad}$.

This variational principle is the usual starting point for any finite element approximations in mechanical modeling.

2.3. *Electromagnetic governing equations*

Considering a microstrip antenna, the electromagnetic governing equations in the V_∞ space and the cavity V consist in the Maxwell's equations and the constitutive relationships. In addition, the boundary conditions, radiation conditions, jump conditions and electromagnetic excitation are considered for the mathematical formulation.

The usual time harmonic approach is considered in the following developments. As a consequence, all field quantities are supposed to be harmonically oscillating functions with a single frequency ω [8], [10].

2.3.1. *The Maxwell equations*

Considering the time-harmonic modeling, the Maxwell's equations can be written in a simplified form in V_∞ and V:

$$\overrightarrow{rot}\,\vec{E} = -j\omega\,\vec{B}, \tag{5}$$
$$\overrightarrow{rot}\,\vec{H} = j\omega\,\vec{D}, \tag{6}$$
$$div\,\vec{D} = \rho, \tag{7}$$
$$div\,\vec{B} = 0, \tag{8}$$

where $\vec{E}$, $\vec{D}$, ρ, $\vec{H}$ and $\vec{B}$ are, respectively, the electric field intensity, the electric flux density, the electric charge density, the magnetic field intensity and the magnetic flux density.

2.3.2. *The constitutive relations*

They describe the macroscopic properties of the mediums.

$$\vec{D} = \epsilon\,\vec{E}, \tag{9}$$
$$\vec{B} = \mu\,\vec{H}, \tag{10}$$

where the constitutive parameters ϵ and μ are, respectively, the permittivity and permeability of the medium. These parameters are scalars for isotropic media.

In the present study, the cavity backed patch antenna is considered to be situated in free space. Then, V_∞ is characterized by the free-space permittivity (ϵ_0) and permeability (μ_0). Moreover, the cavity is supposed to be filled with an homogeneous material represented by its relative permittivity $\epsilon_r = \epsilon/\epsilon_0$ and relative permeability $\mu_r = \mu/\mu_0$. These two properties are here scalars but would have been tensors in the case of inhomogeneous filling material.

2.3.3. *The boundary conditions*

Metallic materials being considered as perfect conductors, the following conditions have to be verified on the ground plane and on the surface of the patch antenna:

$$\hat{n} \wedge \vec{E} = \vec{0}, \tag{11}$$
$$\hat{n}\,.\,\vec{D} = 0, \tag{12}$$

where $\hat{n}$ is the unit normal vector of the considered surface.

2.3.4. *The radiation conditions*

If the outer boundary of a domain recedes to infinity, this domain is called *unbounded* or *open*. In this case, to make sure that the solution of the problem is unique, an additional condition has to be specified at this outer boundary. It is referred to a radiation condition as the Sommerfeld gauge [8]:

$$\lim_{r\to\infty} r\,[\overrightarrow{rot}\,\vec{E} + jk_0\vec{r} \wedge \vec{E}] = \vec{0}, \tag{13}$$
$$\lim_{r\to\infty} r\,[\overrightarrow{rot}\,\vec{H} + jk_0\vec{r} \wedge \vec{H}] = \vec{0}, \tag{14}$$

where k_0 is the free-space wavenumber ($k_0 = 2\pi/\lambda_0 = \omega\sqrt{\epsilon_0\,\mu_0}$).

2.3.5. *The jump conditions*

In the present problem, the conservation laws imply to satisfy the following jump conditions across the interface between the two medias V_∞ and V [11]:

$$\hat{n}\,.\,[\![\vec{D}]\!] = 0, \tag{15}$$
$$\hat{n}\,.\,[\![\vec{B}]\!] = 0, \tag{16}$$
$$\hat{n} \wedge [\![\vec{E}]\!] = \vec{0}, \tag{17}$$
$$\hat{n} \wedge [\![\vec{H}]\!] = \vec{0}. \tag{18}$$

2.3.6. *Electromagnetic excitation*

Studying the antenna scattering, an electric field intensity $\vec{E}^{inc}$ is supposed to appear at a source point of V_∞. It is considered equals to

$$\vec{E}^{inc}(\vec{r}) = \vec{E}_0\,e^{-j\,k_0\,\hat{k}^{inc}.\vec{r}}, \tag{19}$$

where $\vec{E}_0$ and $\hat{k}^{inc}$ are, respectively, the amplitude and propagation vectors (see Figure 3). The analytical expression of $\vec{E}_0$, for a polarization angle denoted α, is given by

$$\vec{E}_0 = \mathbf{R}_{\mathbf{inc}}^{\mathbf{cs}\ T}\,\vec{E}_0^{sph},$$

where $\mathbf{R}_{\mathbf{inc}}^{\mathbf{cs}}$ is the cross matrix between cartesian and spherical coordinates, and $\vec{E}_0^{sph}$ is the electric polarization field in spherical coordinates:

$$\mathbf{R}_{\mathbf{inc}}^{\mathbf{cs}} = \begin{bmatrix} \sin\theta_{inc}\cos\phi_{inc} & \sin\theta_{inc}\sin\phi_{inc} & \cos\theta_{inc} \\ \cos\theta_{inc}\cos\phi_{inc} & \cos\theta_{inc}\sin\phi_{inc} & -\sin\theta_{inc} \\ -\sin\phi_{inc} & \cos\phi_{inc} & 0 \end{bmatrix}$$
$$\vec{E}_0^{sph} = (0\ \cos\alpha\ \sin\alpha)^T.$$

The corresponding magnetic field intensity $\vec{H}^{inc}$ equals to

$$\vec{H}^{inc}(\vec{r}) = \frac{1}{z_0}(\hat{k}^{inc} \wedge \vec{E}_0)\,e^{-j\,k_0\,\hat{k}^{inc}.\vec{r}}, \tag{20}$$

where $z_0 = \sqrt{\mu_0/\epsilon_0}$ is the free space wave impedance.

In the next sections, the usual approach which consists in solving the problem according to $\vec{E}$ is followed. Once $\vec{E}$ is established, the magnetic flux density can be obtained using the first relationship of Maxwell's equations.

2.4. *Weak electromagnetic formulation*

The main difficulty in the resolution of an electromagnetic problem for antennas consists in estimating integrals on an open infinite domain. Using numerical methods such as the Finite Element Method (FEM), the discretized domain to be considered has to be extended far from the source region in order to impose the radiation condition. This leads to huge computing times.

Meanwhile, it is possible to avoid this problem using the Finite Element-Boundary Integral (FEM-BIM) Method [8], first developed in mechanical engineering and later introduced in electromagnetism.

This method consists in introducing a fictitious boundary which encloses the structures to be studied. Interior to this boundary, the FEM is used to formulate the fields, whereas in the exterior region, the fields are represented by a boundary integral. The fields of the two regions are coupled at the fictitious boundary via the field continuity conditions. This leads to a coupled system for solution of the interior and boundary fields.

The analytical developments of this electromagnetic problem are detailed in Jin [8]. The fields formulation in the V_∞ space using the boundary integral method leads to introduce the scalar Green's function G_0.

Then, the weak form of the electromagnetic boundary value problem can be presented in the following formulation [12]:

Find $\vec{E} \in \mathcal{E}_{ad}$ such that

$$F_v(\vec{E}, \vec{E}^*) + F_s(\vec{E}, \vec{E}^*) = F_{ext}(\vec{E}^*) \tag{21}$$

for all admissible electric field $\vec{E}^* \in \mathcal{E}^*_{ad}$, with

$$\begin{aligned}
F_v(\vec{E}, \vec{E}^*) &= \int_V \overrightarrow{rot}\vec{E}^*(\vec{r})\,\frac{1}{\mu_r}\,\overrightarrow{rot}\vec{E}(\vec{r})\,dV \\
&\quad - k_0^2 \int_V \vec{E}^*(\vec{r})\,\epsilon_r\,\vec{E}(\vec{r})\,dV \\
F_s(\vec{E}, \vec{E}^*) &= 2\int_{S_{ap}}\int_{S_{ap}} div\,|_r\,(\hat{n}\wedge\vec{E}^*_s(\vec{r}))G_0(\vec{r},\vec{r}')... \\
&\quad div\,|_{r'}\,(\hat{n}'\wedge\vec{E}_s(\vec{r}'))dS'dS \\
&\quad - 2k_0^2\int_{S_{ap}}\int_{S_{ap}} G_0(\vec{r},\vec{r}')... \\
&\quad (\hat{n}\wedge\vec{E}^*_s(\vec{r})).(\hat{n}'\wedge\vec{E}_s(\vec{r}'))dS'dS \\
F_{ext}(\vec{E}^*) &= -2j\,k_0\int_{S_{ap}}\left(\hat{n}\wedge\vec{E}^*_s(\vec{r})\right)\left(\hat{k}^{inc}\wedge\vec{E}^{inc}\right)\,dS,
\end{aligned}$$

where $S_{ap} = S_{aperture}$ denotes the area of the cavity which is not covered by the antenna (see Figure 2), $\hat{n}$ its unit normal vector, $\vec{E}_s$ the surface electric field and $G_0(\vec{r},\vec{r}')$ is the scalar Green's function, given by [13]–[16]:

$$G_0(\vec{r},\vec{r}') = \frac{e^{-jk_0|\vec{r}-\vec{r}'|}}{4\pi|\vec{r}-\vec{r}'|}$$

Note that the integrals are here reduced to the inside of the cavity and the aperture surface. Nevertheless, the resolution of this weak form, will also give the far fields $\vec{E}^{far}$ and $\vec{H}^{far}$, using the following relationships [4], $\forall\,|\vec{r}| \geq 1/k_0$:

$$\vec{E}^{far}(\vec{r}) = -z_0\left(\hat{k}^{inc}\wedge\vec{H}^{far}(\vec{r})\right), \tag{22}$$

$$\vec{H}^{far}(\vec{r}) = j\frac{k_0}{z_0}\int_{S_{ap}}\mathbb{G}(\vec{r},\vec{r}')\,.\,\left(\hat{n}'\wedge\vec{E}_s(\vec{r}')\right)\,dS', \tag{23}$$

where $\mathbb{G}(\vec{r},\vec{r}')$ is the dyadic Green's function, evaluated for far zone.

Apparently, the functional Eq. (21) only depends on the electric field. Consequently, it may be discretized. However, due to the singularity associated with the derivatives of the Green's function G_0, the evaluation of the surface integral in $F_s(\vec{E},\vec{E}^*)$ leads to a new difficulty.

3. The finite element approximations

This section is dedicated to the finite element approximations.

In the present work, the mechanical behavior of substrate is supposed nonsensitive to the electromagnetic fields. Thus, a weak coupling between electromagnetism and mechanical behavior is assumed. *At each time*, the coupled problem can then be processed in the following two steps:

- First, the mechanical part (Eq. 4) is solved using usual node-based discretization. The mechanical displacement is obtained by interpolating the nodal values of elements.
- Then, the electromagnetic problem (Eq. 21) is solved, taking into account the mechanical strain of the structure.

The specificity of the present method lies in the use of a single finite element having both nodal mechanical and edges electromagnetic degrees of freedom. The mechanical and electromagnetic problems are then solved using the same mesh.

Moreover, the antenna curvatures are time-dependent. This tool allows to predict how the electromagnetic response evolves at each time.

3.1. *Discussion about the finite element shapes*

In order to ensure the solution of the electromagnetic problem to verify the four Maxwell's equations in the three directions, and for a better consideration of electromagnetic boundary condition, the microstrip antenna needs to be discretized using 3D finite elements. For meshes compatibility reasons, the substrate is also discretized using 3D finite elements. Both mechanical and electromagnetic problem are thus solved in the 3D space.

Five main kinds of elements shape can be considered: brick, tetrahedra, prism, pyramid and hexahedra. Brick elements are suited to the study planar structures but they would lead to poor results for warped or distorted antennas, which is our specific study. Indeed, they are not able to automatically mesh arbitrary structures unless staircasing is permitted [4]. Due to their sharp form, the deformed shape of prisms, pyramids and tetrahedral elements are known to lead to nonrealistic stress concentrations in mechanical studies. Finally, the hexahedral elements (or distorted brick element), able to automatically mesh arbitrary structures, are best suited to model the warped antennas.

The finite element approximation of the coupled problem is described in the following subsections.

3.2. *The finite element approximation for the mechanical part*

3.2.1. *Implemented finite element*

The element implemented in the software developed for the present study, is similar to the ANSYS SOLID45 element [17]. It consists in eight nodes linear brick element with three

degrees of freedom at each node (three translations in the nodal directions).

3.2.2. *The elemental matrices*

Here, classical methods are used. Using the engineering formalism, the strain and stress tensors can be written as vectors:

$$\vec{S} = \{S\} = \{S_1 \;\; S_2 \;\; S_3 \;\; S_4 \;\; S_5 \;\; S_6\}^T$$
$$\vec{T} = \{T\} = \{T_1 \;\; T_2 \;\; T_3 \;\; T_4 \;\; T_5 \;\; T_6\}^T$$

Then, the stiffness tensor a can be written as a 6×6 matrix **a**.

Discretizing the studied structure using the FEM, nodal displacements and strains of any element are approximated by

$$\{u\} = \mathbf{N}\{q_e\} \quad \text{and} \quad \{S\} = \mathbf{B}\{q_e\},$$

where the vector $\{q_e\}$ contains the element nodal displacements and **N** and **B** are 6×24 matrices, respectively, containing the interpolation functions and their derivatives.

Substituting these relationships in each integral of the weak formulation (4) restrained to elementary volume V_e and surface S_e, the following elemental stiffness matrix and loads vector are obtained:

$$\mathbf{K}^e = \int_{V_e} \mathbf{B}^T \, \mathbf{a} \, \mathbf{B} \, dV_e,$$
$$\{F^e\} = \int_{V_e} \mathbf{N}^T \{f\} \, dV_e + \int_{S_e} \mathbf{N}^T \{F\} \, dS_e,$$

where $\{f\}$ and $\{F\}$ are vectors containing the body and surface loads applied to the element nodes.

3.2.3. *The discretized problem*

Assembling the elemental matrices over the volume, the mechanical problem can be expressed in the usual following global form:

$$\mathbf{K}\{q\} = \{F_{mecha}\}, \tag{24}$$

where $\{q\}$ contains the mechanical displacement degrees of freedom of the structure and $\{F_{mecha}\}$ corresponds to the applied external mechanical loads.

The stiffness matrix **K** being symmetric and the equation being linear, classical numerical schemes can be used to solve the mechanical problem.

3.3. *The finite element approximation for the electromagnetic part: the use of vector finite elements*

Node-based expansions for finite element solutions are suitable for modeling scalar quantities but typically not so for simulating electromagnetic vector fields. As a consequence, a new approach, recently used in electromagnetism, uses the vector finite elements or *edge elements* which assign degrees of freedom to the edges rather than to the nodes of the elements. These types of elements have been described by Krantz [18]. They have been shown to be free of the shortcomings of node-based expansions [8], [19]. Especially, the occurrence of nonphysical solutions, also called *spurious solutions* and generally attributed to lack of enforcement of the divergence condition is avoided. Several investigations and applications can be found in the literature [4], [7], [19], and [20].

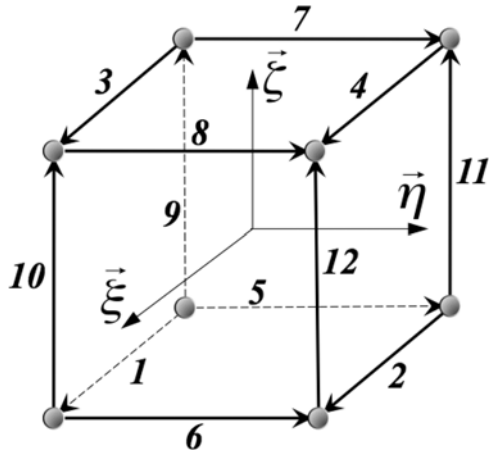

Figure 4. The electromagnetic element.

3.3.1. *Vector finite elements*

The electromagnetic problem represented by the weak formulation (21) will be solved using a classical hexahedral edge element presented in Figure 4.

Here, ξ, η and ζ represent the reduced coordinates, varying in $[-1; 1]^3$, in the $(O, \hat{\xi}, \hat{\eta}, \hat{\zeta})$ system of reference. Each edge is assigned by a number *i*:

- $i = 1$ to 4 for edges parallel to $\hat{\xi}$,
- $i = 5$ to 8 for edges parallel to $\hat{\eta}$,
- $i = 9$ to 12 for edges parallel to $\hat{\zeta}$.

The electrical field in the element is then approximated by

$$\vec{E}^e = \sum_{i=1}^{12} \overrightarrow{W_i^0}(\xi, \eta, \zeta) \, E_i^e. \tag{25}$$

The functions $\overrightarrow{W_i^0}$ are the basis functions and are given in Appendix A. The use of these basic functions leads to the following two important features to be underlined:

- The continuity of the tangential field across all element edges is guaranteed.
- The divergence condition $div \overrightarrow{W_i^0} = 0$ within the element is satisfied.

The Eq. (25) can thus be written in a following matrix form:

$$\vec{E}^e = \begin{Bmatrix} E_x^e \\ E_y^e \\ E_z^e \end{Bmatrix} = \mathbf{W_v}\{E^e\} \tag{26}$$

with

$$\mathbf{W_v} = \begin{bmatrix} \overrightarrow{W_1^0}.\hat{x} & \overrightarrow{W_2^0}.\hat{x} & \dots & \overrightarrow{W_{12}^0}.\hat{x} \\ \overrightarrow{W_1^0}.\hat{y} & \overrightarrow{W_2^0}.\hat{y} & \dots & \overrightarrow{W_{12}^0}.\hat{y} \\ \overrightarrow{W_1^0}.\hat{z} & \overrightarrow{W_2^0}.\hat{z} & \dots & \overrightarrow{W_{12}^0}.\hat{z} \end{bmatrix} \tag{27}$$

and $\{E^e\}$ is the vector of components E_i^e (size 12×1).

Considering the weak formulation Eq. (21), two kinds of terms can be distinguished: terms depending on volume integrals and terms depending on surface ones. All integrals are estimated using the above hexahedral edge element. Meanwhile, it

is necessary to impose one coordinate equals to one for surface integrals. The basis functions $\overrightarrow{W_i^s}$ so obtained are gathered in the $\mathbf{W_s}$ matrix.

3.3.2. *The elemental matrices*

Substituting Eq. (26) into each integral of Eq. (21) restrained to elementary volume V_e and surface S_e gives the following elemental matrices for a curved structure:

$$\mathbf{K_e^v} = \int_{V_e} \mathbf{W_v^T}\,\mathbf{ROT^T}\,\mu_\mathbf{r}{}^{-1}\,\mathbf{ROT}\,\mathbf{W_v^T} dV_e,$$

$$\mathbf{M_e^v} = \int_{V_e} \mathbf{W_v}{}^T\,\epsilon_\mathbf{r}\,\mathbf{W_v}\,dV_e,$$

$$\mathbf{M_e^s} = 2\int_{S_e}\int_{S_e} \mathbf{W_s}{}^T\,\mathbf{N}^T\,G_0(\vec{r},\vec{r}')\,\mathbf{N}'\,\mathbf{W_s}\,dS_e'\,dS_e,$$

$$\mathbf{K_e^s} = 2\int_{S_e}\int_{S_e} \mathbf{W_s}{}^T\,\mathbf{N}^T\,\mathbf{DIV}^T\,G_0(\vec{r},\vec{r}')\,\mathbf{DIV}'\mathbf{N}'\,\mathbf{W_s}\,dS_e'\,dS_e,$$

$$\{F_e^{ext}\} = 2\int_{S_e} \mathbf{W_s}{}^T\,\mathbf{N}^T\,\mathbf{k_w^{inc}}\,\mathbf{R^{cs}}\,\{E_0^{sph}\}\,dS_e,$$

where **ROT** is the rotational operator:

$$\mathbf{ROT} = \begin{bmatrix} 0 & -\partial/\partial z & \partial/\partial y \\ \partial/\partial z & 0 & -\partial/\partial x \\ -\partial/\partial y & \partial/\partial x & 0 \end{bmatrix}. \tag{28}$$

N is the matrix associated to $\hat{n}\wedge .$ with $\hat{n} = n_x\hat{x} + n_y\hat{y} + n_z\hat{z}$:

$$\mathbf{N} = \begin{bmatrix} 0 & -n_y & n_z \\ n_z & 0 & -n_x \\ -n_y & n_x & 0 \end{bmatrix} \tag{29}$$

and **DIV** is the divergence operator, defined by

$$\mathbf{DIV} = \begin{bmatrix} \partial/\partial x & \partial/\partial y & \partial/\partial z \end{bmatrix}. \tag{30}$$

$\mathbf{N}'$ and $\mathbf{DIV}'$ are, respectively, associated to the source point M'. Their expressions are similar to **N** and **DIV**.

3.3.3. *The discretized problem*

Assembling the elemental matrices over the microstrip antenna volume, the electromagnetic problem can be expressed in a very global compact form as follows:

$$\mathbf{Y}\{q_E\} = \{F\}_{emag}, \tag{31}$$

where $\{q_E\}$ contains the electric field degrees of freedom, and

$$\mathbf{Y} = k_0^2(\mathbf{M^v} + \mathbf{M^s}) + (\mathbf{K^v} + \mathbf{K^s}),$$
$$\{F\}_{emag} = jk_0\{F\}^{ext}.$$

$\mathbf{M^v}, \mathbf{M^s}, \mathbf{K^v}, \mathbf{K^s}$ and $\{F\}_{emag}$ are the generalized matrix and vector.

This relationship is similar to the classical static mechanical one. In the electromagnetic case, the *equivalent stiffness matrix* is made of two terms:

- $k_0^2\mathbf{M^v} + \mathbf{K^v}$ which is the contribution of the antenna structure discretized using the FEM.
- $k_0^2\mathbf{M^s} + \mathbf{K^s}$ which is the contribution of the space (containing the electromagnetic sources), discretized using the Boundary Integral Method.

Matrices $\mathbf{M^v}$, $\mathbf{K^v}$, $\mathbf{M^s}$ and $\mathbf{K^s}$ being symmetric and Eq. (31) being linear, its resolution seems to be *easy*. Meanwhile, the evaluation of these last two matrices needs some attention: the green function, which has to be integrated, presents singularities at some particular points of the elements. This difficulty can be avoided using different Gauss points when integrating with respect to surfaces S and S'.

Moreover, $k_0^2\mathbf{M^s} + \mathbf{K^s}$ is a full matrix. In order to reduce computing times, it is converted into a sparse matrix using usual numerical technics [4].

4. Numerical examples

Our numerical tool was validated in Adnet [12]. In this section, it is used to model rectangular microstrip patch antennas, integrated on curved or strained structures. The first two tests deal with curved microstrip antennas on cylindrical and spherical surfaces. In the two last examples, the structure is subjected to mechanical loads. The impact of strains on the microstrip electromagnetic response is discussed.

Considering a scattering problem, the usual output parameter of interest is the RCS in the far field. Indeed, this parameter is an evaluation of the fields scattered from the structure: higher this coefficient is, more detectable is the structure. The RCS scattering is given by Refs. [4], [8]:

$$\sigma = \lim_{r\to+\infty} 4\pi r^2 \frac{|\vec{H}^{sca}|^2}{|\vec{H}^{inc}|^2},$$

where $\vec{H}^{sca}$ is the scattered magnetic field intensity obtained by the far zone expression (Eq. 22).

It is usually represented in logarithmic coordinates and can be normalized with respect to the wavelength λ as follows [4], [8]:

$$\sigma = 10\,log_{10}(\sigma),\ (dBsm),$$
$$\sigma' = 10\,log_{10}\left(\frac{\sigma}{\lambda^2}\right),\ (dB).$$

In the next applications, the influence of microstrip curvatures on electromagnetic performances will be hereafter analyzed through RCS diagrams.

4.1. *A curved microstrip antenna on cylindrical surface*

This test is about a patch antenna inserted in a metallic cylinder (Figure 5). It is vertically illuminated and two kinds of polarizations (vertical $\alpha = 90°$ and horizontal $\alpha = 0°$) are considered. This antenna has been studied by Kempel et al. [22] and Volakis

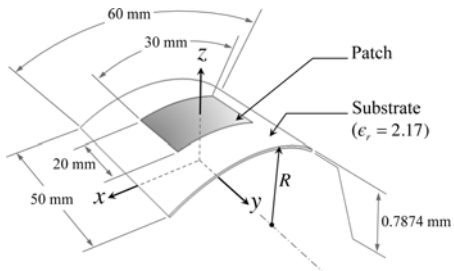

Figure 5. A curved microstrip antenna on cylindrical surface.

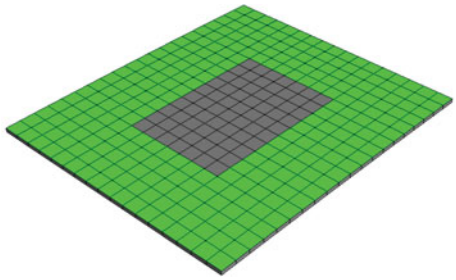

Figure 6. A meshed curved microstrip antenna on cylindrical surface with $R = 2$ m.

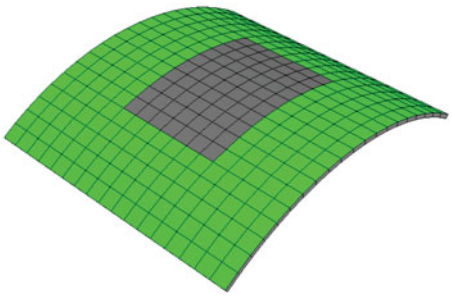

Figure 7. A meshed curved microstrip antenna on cylindrical surface with $R = 0.05$ m.

et al. [4], for several radius values: $R = 0.05$ m, 0.1 m, 0.15 m, 0.2 m and 2 m (the last case being similar to a planar antenna). The authors used cylindrical FE bricks to model the structure. Our meshes, with hexahedral FE for $R = 2$ m and 0.05 m, are shown in Figures 6 and 7.

The monostatic RCS are presented in Figures 8 and 9 for vertical and horizontal polarizations. In spite of the use of different meshes, they are similar with results provided by Kempel et al. [22] and Volakis et al. [4]. The case $R = 2$ m is similar to results obtained with a planar antenna. Near the resonance frequency (5.20 GHz for vertical polarization and 3.62 GHz for horizontal polarization), the level of RCS increases when radius decreases. These simulations show that the scattering of a curved antenna on cylindrical surface is upper than the one of a planar antenna. The antenna is thus failed.

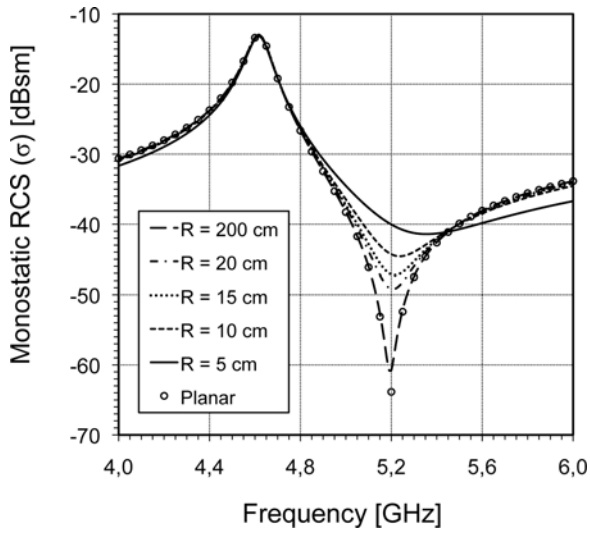

Figure 8. RCS of the antenna on cylindrical surface, vertically illuminated with $\alpha = 90^\circ$.

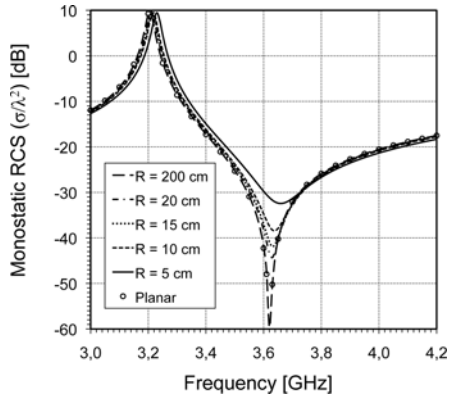

Figure 9. RCS of the antenna on cylindrical surface, vertically illuminated with $\alpha = 0^\circ$.

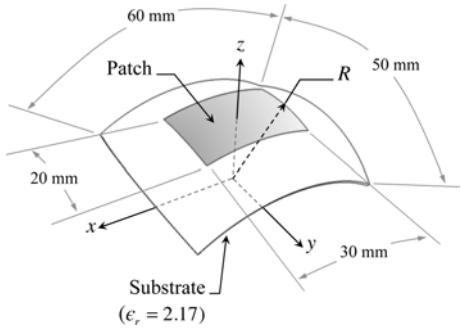

Figure 10. A curved microstrip antenna on spherical surface.

4.2. *A curved microstrip antenna on spherical surface*

In this test, the patch antenna is inserted in a spherical metallic surface (Figure 10). It is vertically illuminated by an incident wave with two kinds of polarizations (vertical $\alpha = 90^\circ$ and horizontal $\alpha = 0^\circ$). Four radius values are considered: $R = 0.05$ m, 0.1 m, 0.2 m and 2 m. Mesh for $R = 0.05$ m is given in Figure 11. The RCS mono static are plotted Figures 12 and 13. Conclusions are similar to the cylindrical case. At the resonance frequency, the antenna scattering strongly depends on the curvature. The antenna again becomes less adapted when R decreases.

The two previous tests deal with antennas on conformal configurations. The simulations show that the ability of hexahedral elements to take into account each node coordinates allows both planar and conformal configurations to be simulated using the same element. This is not true for brick elements: computing planar and conformal cases needs to, respectively, implement two brick elements: a planar element [8] and a curved element [4]. Moreover, the RCS predictions show the influence of the surface curvature on the antenna scattering.

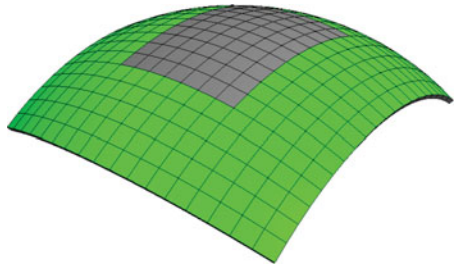

Figure 11. A meshed curved microstrip antenna on spherical surface with $R = 0.05$ m.

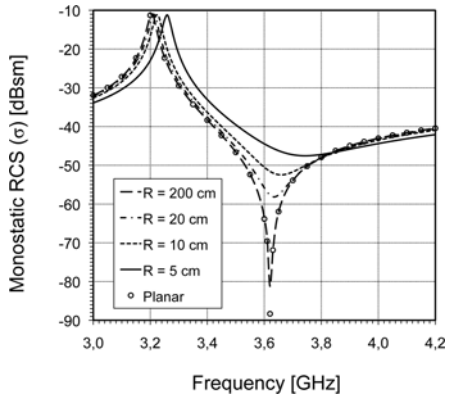

Figure 12. RCS of the antenna on spherical surface, vertically illuminated with $\alpha = 90^{\circ}$.

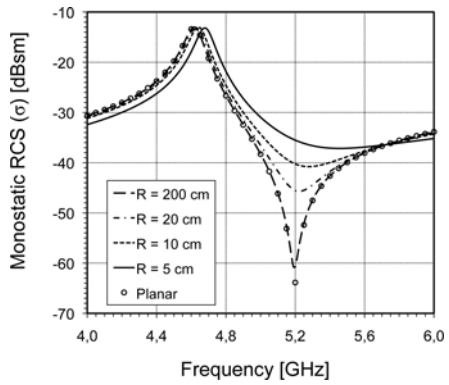

Figure 13. RCS of the antenna on spherical surface, vertically illuminated with $\alpha = 0^{\circ}$.

From these results, the study of mechanical behavior of the antenna and the evaluation of the impact of mechanical strains on the electromagnetic signals must be done. In the next tests, two antennas are considered, subjected to sinusoidal pressure. These simulations need mechanical solution from Eq. (24). The electromagnetism problem (Eq. 31) is solved taking into account the obtained mechanical strain of the structure. As specified previously, the same FE and, consequently the same mesh, are used for mechanical and electromagnetic problems.

4.3. *A strained planar patch antenna*

The following test is about a planar patch antenna, subjected to a sinusoidal pressure (Figure 14). This antenna is supposed to be a 0.03 m × 0.02 m rectangular patch lying on the top of a 0.06 m × 0.05 m × 7.874 10^{-4} m dielectric filled cavity. The dielectric constant and permeability of the filling substrate are $\varepsilon_r = 2.17$ and $\mu_r = 1.00$, and its Young modulus E is about 1 GPa. The structure is clamped at faces defined by $x = -0.03$ m and $x = 0.03$ m. Moreover, the structure is supposed to be vertically illuminated.

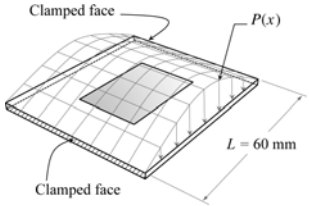

Figure 14. Planar patch antenna under sinusoidal pressure.

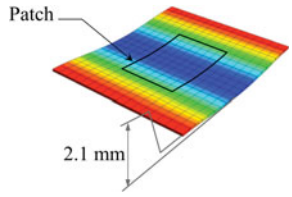

Figure 15. Vertical displacement for $P_0 = 0.025$ N/m^2.

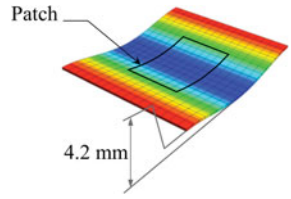

Figure 16. Vertical displacement for $P_0 = 0.05$ N/m^2.

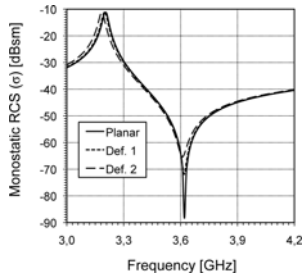

Figure 17. RCS for $P_0 = 0.025$ N/m^2.

The mechanical pressure equals to

$$P(x) = P_0 \left| \sin\left(\frac{\pi\, x}{L}\right) \right|,$$

where L is the length of the dielectric.

The sensitivity of electromagnetic variables is studied for horizontal and vertical polarizations, with respect to two pressure magnitudes: case 1: $P_0 = 0.025$ N/m^2 and case 2: $P_0 = 0.05$ N/m^2.

The maximal vertical displacement value is given in Figure 15 for case 1 and in Figure 16 for case 2. The RCS prediction are plotted Figures 17 and 18. "Def1" and "Def2" means, respectively, results for cases 1 and 2.

The impact of mechanical strains on the electromagnetic behavior cannot be neglected. Especially for case 2, where a 24.7% RCS shift is noticed for a maximal displacement value equals to 0.0042 m. It induces an increasing of the antenna detectability.

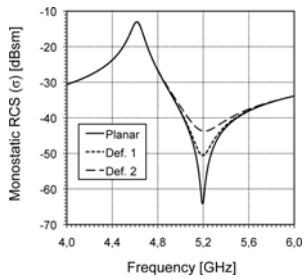

Figure 18. RCS for $P_0 = 0.05$ N/m^2.

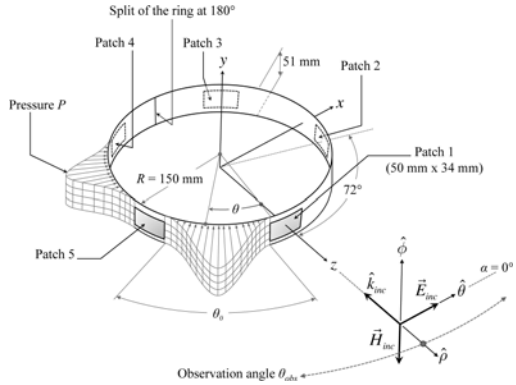

Figure 19. A conformal antenna with five patches on a strained ring.

4.4. *A conformal antenna with five patches on a strained ring*

This last test deals with a conformal antenna made with fives patches, embedded on a ring and subjected to mechanical loads. The geometry of the antenna is given in Figure 19. The thickness of the substrate is 0.8779 10^{-3} m. The angle between two patches equals to 72°. The dielectric constant equals to $\epsilon_r = 2.17$. Its young modulus is 1 GPa. The structure is excited by five cylindrical pressures P which are applied periodically on areas without patches (see two of them Figure 19). Their expression is

$$P(x) = P_0 \sin\left(\frac{\pi\,\theta}{\theta_0}\right), \tag{32}$$

where θ_0 is defined in Figure 19.

The structure is clamped on the lateral face, where $y = -25.5 \times 10^{-3}$ m.

The mesh is presented in Figure 20, and the mechanical displacement induced is given in Figure 21. Maximal displacements are located on the free faces of the antenna and equal to 0.0082 m.

The antenna is vertically illuminated by a planar wave with horizontal polarization. Four frequencies are considered: 0.5 GHz, 1 GHz, 2 GHz and 4 GHz. For each case, bistatic RCS are

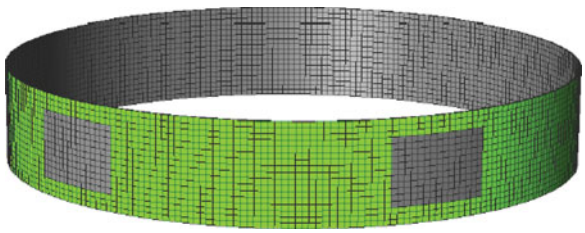

Figure 20. Ring Mesh.

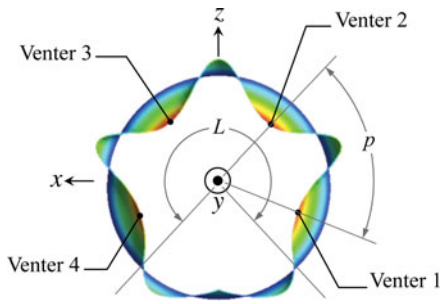

Figure 21. Displacement field of the ring.

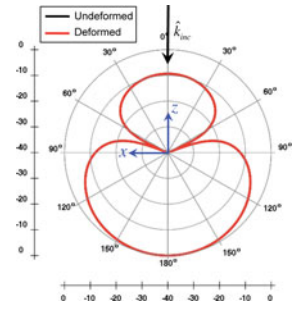

Figure 22. Bistatic RCS for 0.5 GHz frequency.

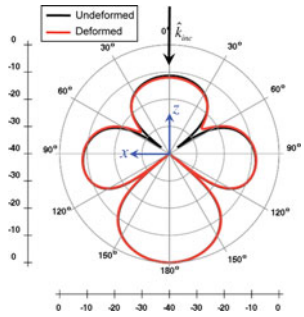

Figure 23. Bistatic RCS for 1 GHz frequency.

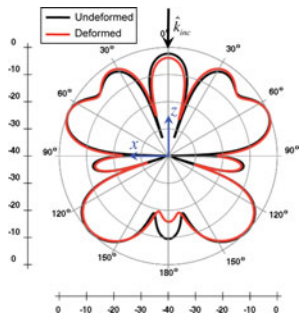

Figure 24. Bistatic RCS for 2 GHz frequency.

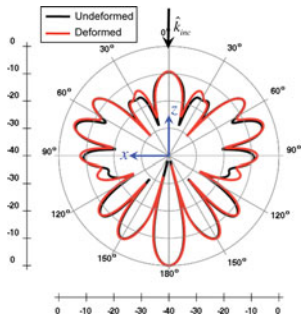

Figure 25. Bistatic RCS for 4 GHz frequency.

plotted Figures 22–25, for initial and strained configurations. The impact of mechanical strains seems to be negligible. This can be explained by the small influence of mechanical displacement on the electrical field plotted Figures 26–29.

In conclusion, in this application, in spite of the maximal value of displacement, the mechanical loads do not affect the RCS curves and the efficiency of the antenna. The antenna is always in good running.

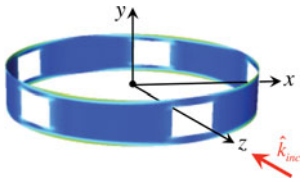

Figure 26. Undeformed case for 0.5 GHz frequency.

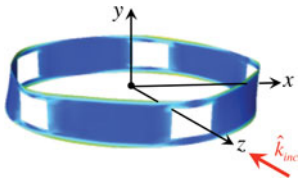

Figure 27. Deformed case for 0.5 GHz frequency.

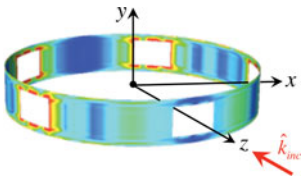

Figure 28. Undeformed case for 4 GHz frequency.

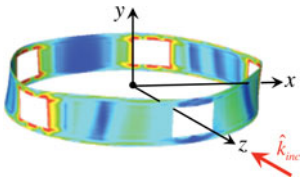

Figure 29. Deformed case for 4 GHz frequency.

5. Conclusion

This work deals with the modeling of the electromagnetic patch antennas subjected to mechanical stresses. It has been motivated by the MSIE project from the competitiveness French Cluster Astech, where the development of metamaterial strip antennas for aeronautical application is evaluated. Such antennas which are thin and conformable can be embedded on any aircrafts surfaces, subjected to mechanical loads. Consequently, the influence of mechanical strains on electromagnetic signals has to be evaluated.

In this way, a recent numerical tool is presented in this paper, taking into account the weak coupling between electromagnetism and mechanical behavior to predict the microstrip antenna scattering. The same hexahedral finite element is developed with a classical nodal formulation for mechanical fields, while the electromagnetic ones are expressed by an edge formulation with vector finite elements.

From the weak formulation, an FEM/BIM approach is used to avoid the discretization of overall space. It consists in introducing a fictitious boundary that encloses the structure to be studied. Classical FEM is used to approximate the fields in the closed domain, whereas the fields in the opened region are evaluated by the BIM.

Then, the 3D finite element developed in this work allows to distort the antenna subjected to mechanical loads and to simultaneously obtain the modified electromagnetic fields (the antenna curvatures are time-dependent).

The numerical simulations presented in this paper show that the distortion of microstrip antenna can affect its scattering. This is the case of the three first examples. Moreover, sometimes, this impact can be negligible even if mechanical displacements are nonzero. For example, in the last test, the maximal displacement of the radius cylinder is close to 5.5%, but simulations show that the antenna is always well running.

Consequently, the study of the coupling between electromagnetism and mechanical behavior is necessary and insightful for antenna scattering. This is also the case for radiative antenna which is the subject of our next work.

References

[1] C.S. You and W. Hwang, "Design of load-bearing antenna structures by embedding technology of microstrip antenna in composite sandwich structure," *Compos. Struct.*, vol. 71, pp. 378–382, 2005.

[2] G.E. Antilla and N.G. Alexopoulos, "Scattering from complex three dimensional geometries by a curvilinear hybrid finite element integral equation approach," *J. Opt. Soc. Am. A*, vol. 11, no. 4, pp. 1455–1457, 1994.

[3] A.K.R.T. Jacobs, "Analysis of planar and curved microstrip antennas," *J. Microwaves Optoelectron.*, vol. 6, no. 1, pp. 96–110, 2007.

[4] J.L. Volakis, A. Chatterjee, and L.C. Kempel, *Finite Element Method for Adn12 Electromagnetics. Antennas, Microwave Circuits and Scattering Application*, New-Jersey: Ant IEEE Press, 1998.

[5] B. Reig, J. Chevrier, A. Lambrecht, J. Greffet, and V. Leconte, *Monaco: Modélisation nano composants*, Poster presentation in J3N2009 Congress, Toulouse, France, 2009.

[6] C. Su, H. Ke, and T. Hubing, "Overview of Electromagnetic Modeling Software," 25th Annual Review of Progress in Applied Computational Electromagnetics, Monterey, California, March 8–12, 2009.

[7] A. Bossavits, *Computational Electromagnetism, Variational Formulation, Complementary, Edge Elements*, San Diego: Academic Press, 1998.

[8] J. Jin, *The Finite Element Method in Electromagnetics*, 2nd ed., New-Jersey: Wiley-Interscience, 2002.

[9] Y.C. Fung, *Foundations of Solid Mechanics*, Englewood Cliffs, New-Jersey: Prentice-Hall, Inc., 1965.

[10] P.P. Silvester and R.L. Ferrari, *Finite Element for Electrical Engineers*, Cambridge: Cambridge University Press, 1990.

[11] L. Demkowicz and L. Vardapetyan, "Modeling of electromagnetic absorption/scatering problems using hp-adaptive finite elements", *Comput. Method. Appl. Mechan. Eng.*, vol. 152, pp. 103–124, 1998.

[12] N. Adnet, *Modélisation numérique du couplage mécanique/électromagnétisme pour l'étude de la sensibilité du comportement électromagnétique d'antennes patch aux déformations mécaniques*, PHD-thesis, Université Paris Ouest Nanterre La Défense, 2012.

[13] C.T. Tai, *Dyadic Green's Function in Electromagnetic Theory*, 2nd ed., New York: IEEE Press, 1993.

[14] T.F. Eibert, J.L. Volakis, D.R. Wilton, and D.R. Jackson, "Hybrid fe/bi modeling of 3-d doubly periodic structures utilizing triangular prismatic elements and an mpie formulation accelerated by the ewald transformation," *IEE Transactions on Antennas and Propagation*, vol. 47, no. 5, pp. 843–850, 1999.

[15] J.L. Volakis, K. Sertel, E. Jorgensen, and R.W. Kindt, "Hybrid finite element and volume integral methods for scattering using parametric geometry," *Comput. Model. Eng. Sci.*, vol. 1, no. 1, pp. 11–24, 2000.

[16] E. Conil, *Propagation électromagnétique en Milieu Complexe*, Ph.D. thesis, Institut National Polytechnique de Grenoble, 2005.
[17] Release 11.0 Documentation for Ansys.
[18] R.G. Krantz and H.R. Parks, *Geometric Integration Theory*, Basel, Switzerland: Birkhauzer Verlag, 2008.
[19] L.S. Andersen and J.L. Volakis, "Adaptive multiresolution antenna modeling using hierarchical mixed-order tangential vector finite elements," *IEE Trans. Antenna. Propagat.*, vol. 49, no. 2, pp. 211–222, 2001.
[20] J.-C. Nédélec, "A new family of mixed elements in r^3", *Numer. Math.*, vol. 50, pp. 57–81, 1986.
[21] T. Özdemir and J.L. Volakis, "Triangular prisms for edge-based vector finite element antenna analysis," *IEE Trans. Antenna. Propagat.*, vol. 45, no. 5, pp. 788–797, 1997.
[22] L.C. Kempel and J.L. Volakis, "Scattering by cavity-backed antennas on a circular cylinder," *IEEE Trans. Ant. Propagat.*, vol. 42, no. 9, pp. 1268–1279, 1994.

Appendix A. The basis functions for the hexahedral edge element

The expression of the shape functions along each edge of the hexahedral element are [4]

$$\overrightarrow{W_k^b}(\xi,\eta,\zeta) = \frac{l_k^e}{8}(1+\eta_k\eta)(1+\zeta_k\zeta)\overrightarrow{grad}\,\xi \text{ for edges parallel to } \vec{\xi},$$

$$\overrightarrow{W_k^b}(\xi,\eta,\zeta) = \frac{l_k^e}{8}(1+\xi_k\xi)(1+\zeta_k\zeta)\overrightarrow{grad}\,\eta \text{ for edges parallel to } \vec{\eta},$$

$$\overrightarrow{W_k^b}(\xi,\eta,\zeta) = \frac{l_k^e}{8}(1+\eta_k\eta)(1+\xi_k\xi)\overrightarrow{grad}\,\zeta \text{ for edges parallel to } \vec{\zeta},$$

where ξ_k, η_k, ζ_k denotes the edge's location in $(O, \hat{\xi}, \hat{\eta}, \hat{\zeta})$ and l_k^e denotes its length.